


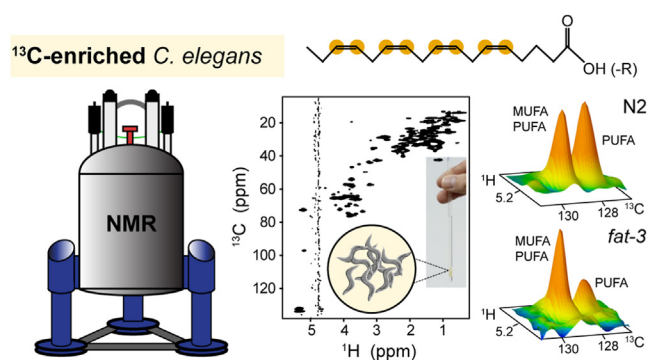
A high-resolution ^{13}C NMR approach for profiling fatty acid unsaturation in lipid extracts and in live *Caenorhabditis elegans*

Bruno Hernández Cravero¹, Gastón Prez¹, Verónica A. Lombardo^{1,2}, Florencia V. Guastaferrri¹ , Carla B. Delprato¹, Silvia Altabe^{1,3}, Diego de Mendoza^{1,3,*}, and Andres Binolfi^{1,4,*} 

¹Institute of Molecular and Cellular Biology of Rosario (IBR-CONICET-UNR), Ocampo y Esmeralda, Rosario, Argentina; ²Center of Interdisciplinary Studies (CEI), National University of Rosario (UNR), Rosario, Argentina; ³Department of Microbiology, Faculty of Biochemical and Pharmaceutical Sciences (FBIOyF), National University of Rosario (UNR) Suipacha 598, Rosario, Argentina; and the ⁴Argentinian Platform of Structural Biology and Metabolomics (PLABEM), Ocampo y Esmeralda, Rosario, Argentina

Abstract Unsaturated fatty acids (UFA) play a crucial role in central cellular processes in animals, including membrane function, development, and disease. Disruptions in UFA homeostasis can contribute to the onset of metabolic, cardiovascular, and neurodegenerative disorders. Consequently, there is a high demand for analytical techniques to study lipid compositions in live cells and multicellular organisms. Conventional analysis of UFA compositions in cells, tissues, and organisms involves solvent extraction procedures coupled with analytical techniques such as gas chromatography, MS and/or NMR spectroscopy. As a nondestructive and nontargeted technique, NMR spectroscopy is uniquely capable of characterizing the chemical profiling of living cells and multicellular organisms. Here, we use NMR spectroscopy to analyze *Caenorhabditis elegans*, enabling the determination of their lipid compositions and fatty acid unsaturation levels both in cell-free lipid extracts and *in vivo*. The NMR spectra of lipid extracts from WT and *fat-3* mutant *C. elegans* strains revealed notable differences due to the absence of Δ -6 fatty acid desaturase activity, including the lack of arachidonic and eicosapentaenoic acyl chains. Uniform ^{13}C -isotope labeling and high-resolution 2D solution-state NMR of live worms confirmed these findings, indicating that the signals originated from fast-tumbling lipid molecules within lipid droplets. Overall, this strategy permits the analysis of lipid storage in intact worms and has enough resolution and sensitivity to identify differences between WT and mutant animals with impaired fatty acid desaturation.  Our results establish methodological benchmarks for future investigations of fatty acid regulation in live *C. elegans* using NMR.

Supplementary key words lipids • physical biochemistry • arachidonic acid • lipids/chemistry • lipid droplets • unsaturated fatty acids • *C. elegans* • solution state NMR spectroscopy • in-cell NMR



Unsaturated fatty acids (UFA) are essential molecules for the normal functioning of cells and multicellular organisms. They are integral components of plasma membranes, serve as energy deposits, and act as signaling molecules that regulate cell growth and animal and plant development (1). Perturbations in UFA homeostasis have been directly linked to the onset of metabolic (2), cardiovascular (3) and neurodegenerative disorders (4).

The nematode *Caenorhabditis elegans* is a powerful model organism to study functions of lipids, including monounsaturated fatty acids (MUFA) and polyunsaturated fatty acids (PUFA) (5). The simple anatomy and wide array of forward and reverse genetic engineering tools available in *C. elegans* makes this model ideal for discovering new roles and regulation for lipid metabolism (6). *C. elegans* is capable of synthesizing all necessary fatty acids (FA) *de novo*, and the core enzymes of fatty acid biosynthesis are conserved,

*For correspondence: Diego de Mendoza, demendoza@ibr-conicet.gov.ar; Andres Binolfi, binolfi@ibr-conicet.gov.ar.

including a range of FA desaturase and elongase activities, enabling *C. elegans* to synthesize 20 carbon omega 6 and omega 3 PUFA, as arachidonic acid (AA) and eicosapentaenoic acid (EPA), respectively (supplemental Fig. S1) (7). Studies in *C. elegans* have characterized numerous pathways that modulate lipid metabolism and fat storage including insulin/insulin-like growth factor, serotonin, and nuclear receptor signals (6). *C. elegans* do not contain adipocytes but store most FA in lipid droplets (LD) (8). These are spherical particles with an outer phospholipids (PL) monolayer that surrounds a core of neutral lipids, mainly triacylglycerols (TAG) molecules and low amounts of free FA, cholesterol, and cholesterol esters (9). LD modulate *C. elegans* energy balance and are involved in lipid homeostasis and lifespan control in *C. elegans* (10).

To better understand the mechanisms by which lipid physiology is regulated in *C. elegans*, it is essential to develop methods for characterizing the dynamics of FA metabolism in live animals. Conventional lipid analysis is commonly performed by solvent extraction-based methods coupled to GC/MS (11), which are typically destructive and time consuming. Moreover, information linking cellular dynamics and functionality is often lost during extraction steps making them less useful for understanding the fundamental biological processes that are needed for controlling UFA homeostasis. Although fixative stains such as Oil Red O or Nile Red measure distributions of lipid-like species across tissues (12), these fluorescent probes cannot provide detailed chemical information about FA compositions, degrees of unsaturation and chain lengths. Coherent anti-Stokes Raman spectroscopy (CARS) is also a powerful methodology to study the distributions of lipid-rich particles, including LD, in live worms but information about individual lipid species is not straightforward (13–15). Thus, studying UFA compositions at high resolution in multicellular organisms is difficult to accomplish with existing methods.

Unlike other analytical tools, solution state NMR spectroscopy is nondestructive and has been extensively applied to characterize the lipid composition of oils and fats (16–18), tissue extracts (19, 20), body fluids (21, 22) and isolated lipoparticles (23), in a tag-free manner and in quantitative terms (24). Furthermore, high resolution, heteronuclear 2D NMR methodologies allowed determining the speciation of UFA and positional analysis of double bonds along the acyl chains (20, 25).

Notably, NMR has been used to characterize biomolecules with high resolution in multicellular organisms. By introducing ^{13}C -isotope enrichment in the water flea *Daphnia magna*, metabolic compositions were analyzed using 2D ^1H - ^{13}C correlation NMR spectra, thus expanding the number of compounds that can be identified and analyzed compared with standard ^1H NMR metabolomics studies (26, 27). Other applications of multidimensional, solution state NMR spectroscopy

studies in live animals include the monitoring of endogenous enzymatic activities (28) and protein conformation and dynamics in zebrafish (*Danio rerio*) oocytes (29) and embryos (30). Recently, Park et al. applied NMR spectroscopy on live, ^{13}C isotopically enriched *C. elegans*, to characterize time-dependent metabolic changes of WT and mutant worms with impaired AMP-activated kinase activity, a central regulator of cellular metabolism (31). While these studies demonstrate the advantages of NMR spectroscopy to perform metabolic studies in live multicellular organisms, its application is still not widespread. This includes the high resolution analysis of lipid compositions.

Here, we used uniform ^{13}C isotope labeling followed by multidimensional solution state NMR spectroscopy to identify the UFA compositions of WT (N2) and mutant *C. elegans* strains with impaired PUFA biosynthesis. We show that NMR sensitivity and resolution permits the determination of unsaturation levels of *C. elegans* fatty acyl chains and analysis of lipid storage both in cell-free lipid extracts and live worms. Our results provide a methodological framework to characterize genetic, environmental, dietary, and pharmacological effects on lipid composition and biosynthesis.

MATERIALS AND METHODS

Reagents

Buffers, salts, and chemicals were reagent grade and were used without further treatments. Unless specified, all reagents were purchased from Merck or Sigma-Aldrich. Pure oleic acid, linoleic acid (LA), di-homo- γ -linolenic acid, AA acid, triolein and phosphatidylcholine [16:0/18:2(n-6)] were from Sigma-Aldrich. They were dissolved in deuterated chloroform (CIL, USA) and used immediately without further treatment.

Nematode strains

C. elegans strains used in this work were obtained from the *Caenorhabditis* Genetics Center, University of Minnesota (<https://cgc.umn.edu/>). We used Bristol N2 (WT) and the single mutants, $\Delta 6$ fatty acid desaturase (*fat-3*) (*ok1126*) and *fat-4* (*ok958*). Worms were routinely propagated on nematode growth medium (NGM) agar plates supplemented with 13 μM cholesterol and seeded with *Escherichia coli* OP50 according to standard procedures (32).

Sample preparation for in vivo NMR experiments

To obtain uniformly ^{13}C -isotopically enriched N2 (Bristol) and *fat-3(ok1126)* *C. elegans* samples, agar plates were spread using 10X pellet of an overnight culture of *E. coli* NA22 (33) grown in a M9 minimal medium supplemented with 2 g/L of ^{13}C -D-glucose (Cortecnet, France) and 1 g/L of ^{14}N -ammonium chloride (Merck) as sole carbon and nitrogen sources, respectively. Typically, each worm NMR sample requires 50 ml of a saturated, ^{13}C -isotopically enriched NA22 culture. Next, 60,000 L1s worms from eggs prepared by

bleaching (34) were grown on 15 ml NGM plates seeded with 1 ml concentrated *E. coli* NA22 to L4 state. Non-isotopically enriched NMR samples were prepared using *E. coli* OP50 cultured in Luria-Bertani broth.

All *C. elegans* strains were synchronized and analyzed at the L4 stage. We use this procedure so as to detect differences that arise from the activity of FAT-3 and not from different lipid storage/consumption rates that may depend on a particular developmental stage. Synchronized L4 worms were collected in a 15 ml falcon tube, centrifuged for 2 min at 2000 g to remove media and washed twice on M9 buffer to remove bacteria. We then discarded the supernatant, added M9 buffer to complete a volume of 700 μ l and supplemented this solution with 77 μ l of D₂O (99.9%). Worms were gently resuspended with a cut pipette tip, loaded in a 5 mm NMR Shigemi tube (without applying the plunge) and decanted to the bottom by gentle spinning. All NMR experiments were performed using 40,000–60,000 L4 worms. Worms were counted during the last wash step. We suspended them in 10 ml of M9 media, took three aliquots of 5 μ l, place them on a glass slide and counted the number of worms in each drop under the microscope. We calculated the mean number from the three drops and multiplied it by 2,000 to obtain the total number of worms.

C. elegans lifespan analysis

Worm's lifespan during NMR acquisitions was assessed on paralleled, independent samples by removing small aliquots of the worm suspension from the NMR tube at 2, 4, 6, and 9 h after the experiments started. Worms were then transferred to fresh NGM plates where we counted the live and dead ones to obtain the survival percentages at each time point. Viability was determined by spontaneous and/or touch-induced movement. All observations were performed on an Olympus MVX10 with 10X and 40X magnifications. Images were taken with an Olympus DP72 camera. Each assessment was done in triplicates.

Lipid extraction

To extract lipids from whole worms, we used an adaptation of the protocol reported by Folch et al. (35). Lipid extracts were made from pellets of 40,000 frozen worms previously grown at 20°C. In all cases; worms were synchronized at L4 stage and frozen before lipid extraction. Pellets were thawed, washed with M9 buffer, resuspended in 1.3 ml pure methanol, and sonicated on ice 3 times for 30 s at maximum power (Branson Sonifier). We waited for 2 min between each sonication cycle to avoid sample heating. After sonication, we added 2.6 ml of chloroform and 1.3 ml 0.5 M KCl/0.08 M H₃PO₄ to a final ratio of 1:2:1. Afterward, solutions were sonicated in an ultrasonic water bath for 15 min, vortexed twice for 1 min and centrifuged for 10 min at 2,000 g to induce phase separation. The lower, hydrophobic phase was collected into a clean glass tube, dried under constant nitrogen stream, resuspended in 500 μ l of deuterated chloroform supplemented with 0.005% butylated hydroxytoluene (Sigma-Aldrich) to prevent lipid oxidation and filled into 5 mm NMR tubes (Norell, USA) with a glass pipette.

GC/MS experiments

FA composition of N2 (Bristol) and *fat-3* (*ok1126*) nematodes was determined by GC-MS, as previously described (36). Lipids extracts were prepared using similar protocols as for NMR

experiments. Fatty acid methyl esters (FAMES) were prepared by incubating lipid samples with 1%–2% concentrated sulfuric acid in methanol for 2 h at 80°C. FAMES were extracted with hexane (2 ml), evaporated to dryness, and then dissolved in hexane. GC/MS was done using a Shimadzu GC-2010 Plus instrument equipped with a SUPELCOWAX-10 (Sigma-Aldrich) 100% polyethylene glycol column. The helium flux was 1 ml/min, and the heating program was 180°C (0 min–32 min), and then a gradient increasing 3°C/min from 180°C to 240°C. The split was 1/30 and the ionization voltage was 70 eV with an ionic range from 50 to 600 Da. The ion specters were registered as relative abundance in function of mass/charge (*m/z*). Peak assignment was done using the mixture of standards of FAMES AGS Supelco (Sigma-Aldrich). The quantification of UFA was performed using GC/MS and expressed as a percentage of the total FA.

Fluorescence microscopy

Samples were prepared by following previously established routines (37). Briefly, N2 (Bristol) worms were harvested, transferred to an eppendorf tube, and washed twice with PBS supplemented with 0.01% of Triton X-100. Worm pellet was fixed with 150 μ l of 40% isopropanol for 3 min. In the meantime, a fresh Nile Red staining solution was prepared by adding 6 μ l of Nile Red stock (500 μ g/ml in acetone) to 1 ml of 40% isopropanol and was kept in the dark until it was used. After fixing the worms, the supernatant was removed and 150 μ l of the freshly prepared Nile Red staining solution was added. The sample was incubated at room temperature for 2 h in the dark with gently shaking. Worms were washed with 1 ml of M9 buffer, supernatant was removed, and worms were resuspended in 50 μ l of M9. Subsequently, 5 μ l of worm suspension was mounted on a slide for fluorescent microscopy imaging. Images were obtained with a Nikon Eclipse 800 fluorescence microscope using a USH-103 mercury lamp, filtered at 540 nm/620–660 nm (excitation/emission) for PL detection, and at 488 nm/510–560 nm (excitation/emission) for TAG detection (38). All images were processed with ImageJ (<https://imagej.net/ij/>) (39).

NMR experiments

All NMR experiments were recorded on Bruker 600 MHz Avance II, and 700 MHz Avance III spectrometers equipped with triple resonance inverse NMR probes (5 mm ¹H/¹³C/¹⁵N TXI).

- (a) NMR experiments of lipid extracts in deuterated chloroform: 1D ¹H spectra were recorded using a pulse sequence with a 30° flip angle hard pulse (*zg30*), a fid resolution of 0.43 Hz, 64 scans, and 20 ppm spectra width (SW). Processing was done using an exponential window function multiplication (EM) with line broadening (LB) of 0.1 Hz, Fourier transform, and baseline correction. 2D ¹H–¹H total correlation spectroscopy was acquired using the MLEV sequence for mixing (*mlevqpphprzf*) with a mixing time of 60 ms and spinlock 9.2 KHz. We acquired 16 scans and 2K/256 increments in the direct and indirect dimensions, respectively, for a SW of 12 ppm. Spectra were processed with sine-bell window function multiplication and baseline correction. Full spectral range, 2D ¹H–¹³C heteronuclear single quantum coherence (HSQC) spectra of free UFA and lipid extracts were acquired with a phase-sensitive pulse sequence and gradient pulses (*hsqcqpph*). We used 1K and 256 increments in ¹H and ¹³C dimensions,

respectively (resolution of 21.8 Hz and 220.1 Hz), 16 scans and 16 ppm (^1H) and 160 ppm (^{13}C) SW. ^{13}C decoupling was accomplished with the GARP sequence. Processing was done using sine-bell window function multiplications, Fourier transform, and baseline correction in both dimensions. For semiselective 2D ^1H - ^{13}C HSQC's of natural abundance lipid extracts we used the same pulse sequence and folded signals were removed using digital quadrature detection as previously described (20). NMR parameters were 1,024 and 512 increments in ^1H and ^{13}C , respectively (resolution 4.1 Hz and 2.75 Hz), 40 scans and SW of 3 ppm (^1H , 5.4 ppm offset) and 4 ppm (^{13}C , 129.5 ppm offset). Processing was done with EM and baseline correction. These spectra were collected with non-isotopically enriched samples. For semiselective, 2D ^1H - ^{13}C HSQC's of ^{13}C -isotopically enriched lipid extracts we used an HSQC pulse sequence with a ^{13}C selective excitation pulse centered on the UFA region (129 ppm) and with heteronuclear and homonuclear decoupling schemes to minimize ^{13}C - ^{13}C coupling (40).

- (b) NMR experiments of live *C. elegans*: 1D ^1H spectra of live worms and leakage control spectra in aqueous M9 media were acquired using a pulse sequence with excitation sculpting for water suppression (*zgpg30*) (41). We used a resolution of 2.72 Hz, 128 scans, and 16 ppm SW. Processing was carried out with EM (LB 5Hz) and baseline correction. For 1D ^{13}C spectra, we used a pulse sequence with a 30° flip pulse and inverse gated decoupling (*zgpg30*). Fid resolution was 1.63 Hz, NS 256, and 300 ppm SW. Processing was carried out with EM (LB 30 Hz) and baseline correction. Full spectral range, 2D ^1H - ^{13}C HSQC spectra of live worms with uniformly, ^{13}C -isotopic enrichment were acquired with a sensitivity-enhanced pulse sequence (*hsqcetgpsisp2.2*). We used 2K and 256 increments in ^1H and ^{13}C dimensions, respectively (resolution of 10.9 Hz and 206 Hz), 4–8 scans and 16 ppm (^1H) and 150 ppm (^{13}C) SW, experimental time was 36 min and ^{13}C decoupling was achieved with the GARP sequence. Processing was done using sine-bell window function multiplications, Fourier transform, and baseline correction in both dimensions. Semiselective experiments on live ^{13}C -enriched worms were acquired with heteronuclear and homonuclear decoupling schemes. We used 2K and 256 increments in ^1H and ^{13}C dimensions, respectively (resolution of 10.26 Hz and 8.25 Hz), 16 scans and 16 ppm (^1H) and 6 ppm (^{13}C) SW. Spectra were processed using q sine-bell window function multiplication and baseline correction.

Lipid chemical shifts were obtained from reference spectra recorded in this work, from previous articles (19–22, 24, 25, 42) and from The American Oil Chemists' Society Lipid Library (<https://lipidlibrary.aocs.org/>). Relative lipid quantifications of N2 (Bristol) and *fat-3* (*ok1126*) chloroform extracts were done by integration of ^1H signals corresponding to different lipid groups and referenced to the integral value of the terminal methyl region, referred to the total lipids (TL) signal, as previously reported (24). In all cases, the number of contributing spins for each group of signals was considered. For instance, for UFA quantifications we used the signal corresponding to the CH_2 group at position -1 from the insaturations ($-\text{CH}_2-\text{CH}=\text{CH}-$) and for TAG the signal corresponding to the $\text{C}\beta$ backbone glycerol group ($-\text{CHOR}$), using the formulas $\text{UFA}\% = (3I_{\text{CH}_2-\text{CH}=\text{CH}}/4I_{\text{CH}_3}) \times 100$ and $\text{TAG}\% = (3I_{\text{CHOR}}/I_{\text{CH}_3}) \times 100$ (24). The same strategy was used for other lipid species reported. Integrations were done using the standard integration tool in Topspin 3.5 (<https://www.bruker.com/en/products-and-solutions/mr/nmr-software/topspin.html>) on predefined spectral regions. In all cases the upper and lower limits of integration regions were chosen on local minima. Signal volume ratios from 2D ^1H - ^{13}C HSQC spectra of live N2 and *fat-3* worms and worm extracts were calculated by integrating each signal using Sparky (<https://www.cgl.ucsf.edu/home/sparky/>) (43), dividing the *fat-3* values from those of N2 and using the signal from the methyl groups for normalization. Statistical analysis was done with Sigma Plot (<https://systatsoftware.com/>). We used Student's t tests for comparison between the means of N2 and *fat-3* lipid ^1H NMR signals, and one-way ANOVA for 2D ^1H - ^{13}C HSQC lipid signal ratios. Acquisition and processing of the NMR spectra were performed using Topspin 3.5 (Bruker BioSpin; <https://www.bruker.com>). The 2D spectra analysis and visualization was done with Sparky (43).

RESULTS

NMR analysis of *C. elegans* lipid extracts

To demonstrate the suitability of solution state NMR spectroscopy to characterize the lipid composition of *C. elegans*, we first recorded 1D ^1H and 2D ^1H - ^{13}C HSQC spectra of N2 lipid extracts (Fig. 1). We directly compared these spectra with those from pure lipid species and assigned most of the ^1H and ^{13}C resonances present in the spectra (Fig. 1 and supplemental Fig. S2). We clearly detected signals from the different atoms of UFA, PL, TAG and other lipids, including diacylglycerols and cyclopropane fatty acids. Inspection of the olefinic $-\text{CH}=\text{CH}-$ correlations at 5.35 ppm in the ^1H dimension of the ^1H - ^{13}C HSQC spectrum of N2 extract showed two well-defined signals in the ^{13}C dimension centered at c.a. 128.5 and 130.5 ppm (Fig. 1C). Comparison with reference MUFA and PUFA spectra revealed that the lower field signal (130.5 ppm) arise from the combined contribution of MUFA and PUFA while the upper field one (128.5 ppm) is composed solely from PUFA atoms (inset Fig. 1C), in agreement with previously published UFA chemical shifts values (20).

While the 2D ^1H - ^{13}C HSQC spectrum of lipids allows differentiating PUFA from total UFA, the resolution is not enough to resolve signals from individual UFA acyl chains. Accordingly, we acquired 2D ^1H - ^{13}C semiselective HSQC spectra of N2 lipid extracts and pure UFA samples (Fig. 2). This methodology substantially increases the resolution of selected spectral regions and was previously applied to analyze individual or discrete groups of UFA in body fluids and lipid mixture (20, 25). We showed that the original downfield and upfield signals in the full range ^1H - ^{13}C HSQC spectra are composed of multiple signals that can be resolved and assigned to specific groups of UFA acyl chains (Fig. 2). These results indicate that NMR is suitable to analyze the lipid compositions of *C. elegans* extracts, including

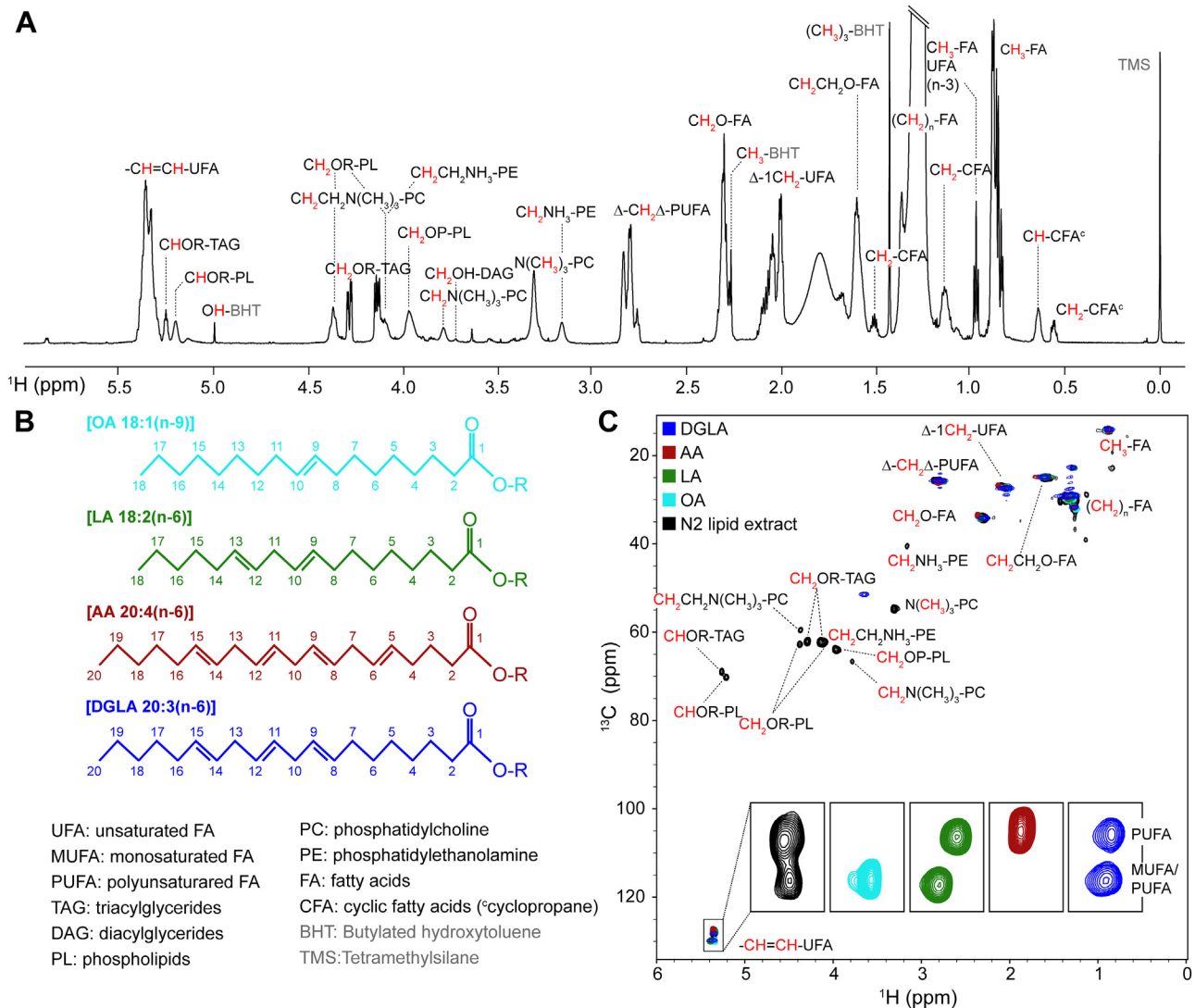


Fig. 1. NMR signal assignment of *Caenorhabditis elegans* lipid extracts. A: ID ^1H NMR spectrum of N2 lipid extract. Assignments are included on top of each signal and the contributing proton(s) is indicated in red. B: Schematic representation of several UFA, including MUFA (OA) and PUFA (LA), (AA) and (DGLA). C: 2D ^1H - ^{13}C HSQC spectra of N2 lipid extract and the UFA depicted in panel (B). Assignments are indicated and the proton(s) and carbon contributing to each signal are identified in red. All 2D ^1H - ^{13}C HSQC spectra were acquired at natural abundance of ^{13}C . UFA, unsaturated fatty acids; DGLA, di-homo- γ -linolenic; LA, linoleic acid; HSQC, heteronuclear single quantum coherence; OA, oleic acid; AA, arachidonic acid.

the characterization of different degrees of unsaturation in the UFA acyl-chains.

To test this hypothesis we used NMR to analyze the UFA content of lipid extracts of the WT (N2) strain and the *fat-3* mutant lacking the $\Delta 6$ FA desaturase FAT-3. This enzyme catalyzes the rate limiting step in the conversion of linoleic LA and α -linolenic acid (ALA) FA into C20 PUFA (supplemental Fig. S1). Thus, *fat-3* worms do not synthesize PUFA that uses as a substrate LA and ALA being deficient in several FA including C20 AA and EPA (7). Comparison of ID ^1H spectra of N2 and *fat-3* worm lipid extracts showed differences in spectral regions corresponding to UFA protons (Fig. 3A). As expected, signals of bis-allylic ($-\Delta\text{CH}_2\text{-}\Delta$, ~ 2.8 ppm) protons, which correspond exclusively to PUFA were less intense in *fat-3* mutants. Inspection of

the signals corresponding to ^1H at position -1 from the insaturations ($\Delta\text{-1CH}_2$, ~ 2 ppm) revealed lower amounts of PUFA and higher amounts of MUFA and LA and ALA, suggesting that these species, which are the substrates of FAT-3 desaturase, accumulate in these animals, in agreement with previous observations (7). GC/MS experiments performed under similar experimental conditions confirmed these observations (supplemental Table S1). Further analysis of the ^1H spectrum of *fat-3* worm extract showed that TAG signals were also lower compared to N2. This was evident from the $-\text{CHOR}$ and $-\text{CH}_2\text{OR}$ signals corresponding to the glycerol backbone protons. Peak integration and relative quantification of the different lipid groups confirmed that UFA levels were higher while TAG were lower in *fat-3* extracts compared to N2

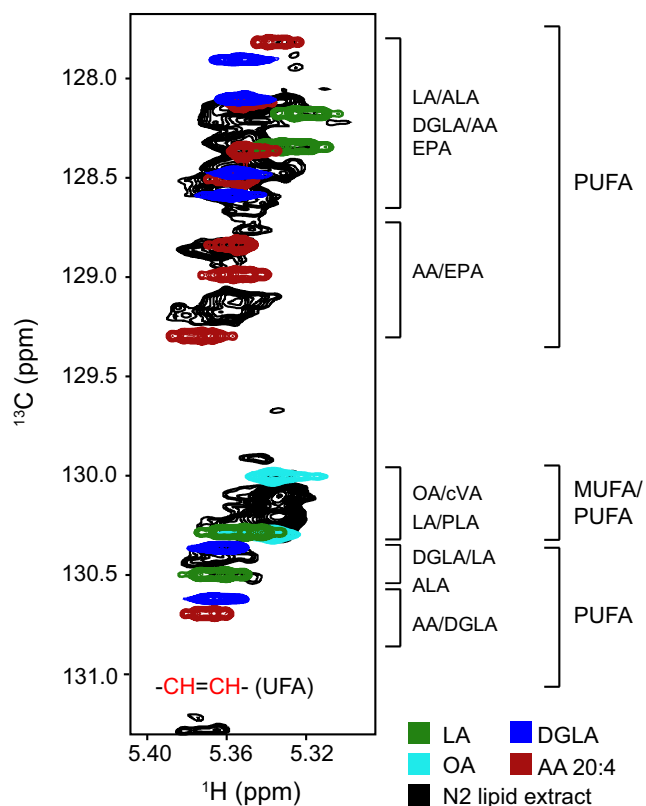


Fig. 2. NMR identification of *Caenorhabditis elegans* UFA. Overlaid of natural abundance semiselective ^1H - ^{13}C HSQC spectra of N2 lipid extract (black) and pure fatty acids OA (cyan), LA (green), DGLA (blue), and AA (burgundy). Signals from the different UFA are indicated on the right. UFA, unsaturated fatty acids; AA, arachidonic acid; ALA, α -linolenic acid; cVA, cis-vaccenic acid; DGLA, di-homo- γ -linolenic; EPA, eicosapentaenoic acid; LA, linoleic acid; HSQC, heteronuclear single quantum coherence; OA, oleic acid; PLA, palmitoleic acid.

(supplemental Table S2). We also noted that PL content was higher in *fat-3* animals. Direct quantification of PUFA using the 1D ^1H NMR integrals and equations is not possible because the absolute number of protons that contribute to the bis-allylic signal ($-\Delta\text{-CH}_2\text{-}\Delta$, ~ 2.8 ppm) cannot be determined as it depends on the number of unsaturation in each PUFA (19). However, integration ratios of non-overlapped NMR signals may provide information about relative lipid levels between N2 and *fat-3*. Accordingly, we recorded natural abundance 2D ^1H - ^{13}C HSQC spectra on N2 and *fat-3* extracts. Spectra overlay showed lower PUFA and TAG signal intensity in *fat-3* samples (Fig. 3B). Integration and calculation of the volume ratios between *fat-3* and N2 corroborated the visual analysis (inset Fig. 3B). This was clearly observed for the $\Delta\text{-CH}_2\text{-}\Delta$ and the upfield component of the olefinic ($-\text{CH}=\text{CH}-$) regions that correspond exclusively to PUFA, and for the TAG signal in the $-\text{CHOR}$ region.

Compared to N2, the semiselective ^1H - ^{13}C HSQC spectra of the olefinic $-\text{CH}=\text{CH}-$ region of *fat-3* worms revealed the presence of MUFA and the $\Delta 6$ desaturase substrates, LA and ALA and an overall deficiency in

other PUFA, most notably virtually undetectable levels of AA and EPA (Fig. 3C). A complementary analysis of *fat-4* mutants that synthesize di-homo- γ -linolenic and eicosatrienoic [20:4(n-3)] acids, but is unable to synthesize either AA or EPA (supplemental Fig. S1) due to a deficiency in $\Delta 5$ desaturase, allowed us to assign a selected group of NMR signals that belong exclusively to these PUFA (5.36 and 128.85–129.3 ppm in ^1H and ^{13}C , respectively) (supplemental Fig. S3). Moreover, the specific positions of other UFA can be inferred by identifying signals that are present or absent in the different mutants. For instance, the carbon signals between 130 and 130.3 ppm in the lower lobe, present in all of the spectra belong to MUFA, LA, and ALA. With a similar rationale the signals between 128.1 and 128.6 ppm in the upper lobe, present in N2, *fat-3* and *fat-4* should arise from LA and ALA. This analysis is in agreement with previous UFA assignments (20, 25) and while it might not be absolute in complex mixtures due to the overlap of individual UFA signals, it provides enough resolution to detect changes in UFA pools and assign them to restricted set of acyl chains. Overall, these results show that NMR is a useful tool to delineate and quantify lipids of *C. elegans* extracts and that the double bond region of ^1H - ^{13}C HSQC spectra represents a powerful fingerprint to identify changes in UFA composition, including positional analysis of lipid unsaturation.

Lipid detection in ^{13}C , uniformly enriched live *C. elegans*

Solution state NMR of *C. elegans* extracts enabled the dissection of lipid compositions in cell-free lipid extracts including the analysis of UFA chains. Next, we explored the use of NMR for the analysis of UFA in live ^{13}C -isotopically enriched *C. elegans*. Uniform isotope labeling in *C. elegans* is a simple and inexpensive procedure that entails feeding worms with *E. coli* cultured in the presence of ^{13}C -D-glucose as the sole carbon source (Fig. 4A), resulting in ^{13}C uniformly enriched worms (31). Comparison of 2D ^1H - ^{13}C HSQC NMR spectra of isotopically enriched worms or at natural abundance of ^{13}C showed that isotope labeling increases the overall sensitivity and allowed us to record 2D ^1H - ^{13}C HSQC spectra with excellent signal-to-noise ratios in ~ 30 min (Fig. 4B, C). Replicate experiments on independent ^{13}C -isotopically enriched worm samples produced very similar results (supplemental Fig. S4A, B). As expected, increasing the number of worms in the receiver coil volume of the NMR tube resulted in proportional signal intensity increase (supplemental Fig. S4A). This information is useful to derive normalization factors for 2D ^1H - ^{13}C HSQC analyses if one wishes to compare samples with different number of worms. Comparison of the 1D ^1H spectrum of live *C. elegans* grown on non-isotopically enriched OP50 and NA22 cells showed no significant changes in major lipid resonances (supplemental Fig. S4C),

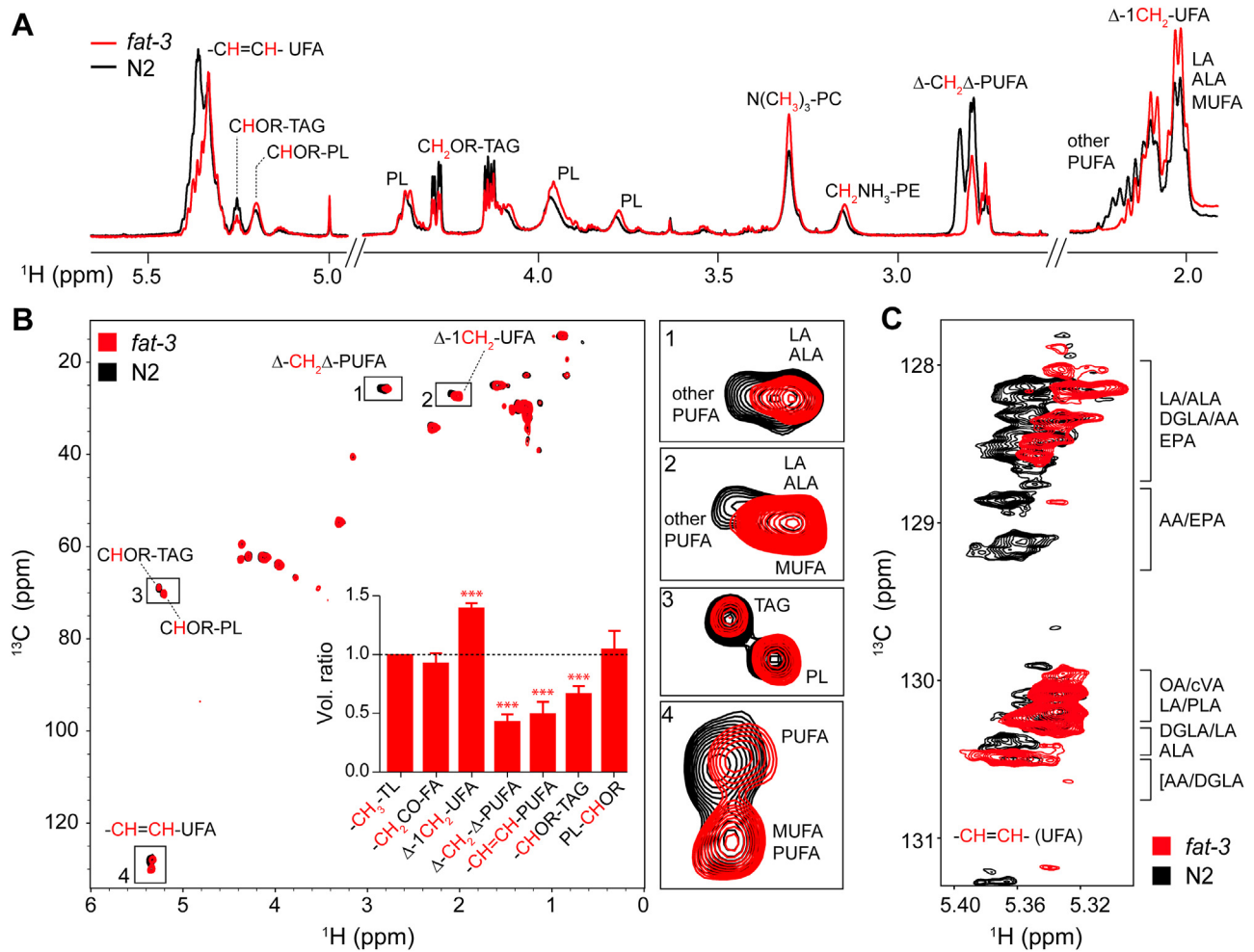


Fig. 3. NMR analysis of N2 and *fat-3* worm lipid extracts. A: ID ^1H NMR spectra of lipid extracts of N2 (black) and *fat-3* (red) in the olefinic and aliphatic region. Signals corresponding to different lipid species are annotated. B: ^{13}C natural abundance 2D ^1H - ^{13}C HSQC spectra of N2 and *fat-3* lipid extracts. Numbered boxes indicate the signals of atoms from different lipids and are enlarged in the individual panels on the right. These correspond to the bis-allylic CH_2 groups ($\Delta\text{-CH}_2\Delta\text{-PUFA}$) (region 1), the CH_2 groups at position -1 from the insaturations ($\Delta\text{-1-UFA}$) (region 2), the backbone $-\text{CHOR}$ group of TAG and PL (region 3) and the olefinic CH groups of UFA ($-\text{CH}=\text{CH}-\text{UFA}$) (region 4). Inset shows the cross-peak volume ratio between *fat-3* and N2 lipid signals. Bar graph represents mean and std. dev. of three determinations on independent samples. Significant difference between N2 and *fat-3* lipid groups, $***P < 0.001$. C: Natural abundance 2D ^1H - ^{13}C semiselective HSQC spectra registered in the olefinic ($-\text{CH}=\text{CH}-$) region highlighted in region 4. Assignments from different UFA signals are indicated. UFA, unsaturated fatty acids; HSQC, heteronuclear single quantum coherence; TAG, triacylglycerols; PL, phospholipids.

confirming that the large differences in signal amplitude observed in Fig. 4B, C arise mainly from the incorporation of ^{13}C in the animals. Leakage analysis after 9 h showed only few, low-intensity peaks corresponding to low-molecular weight metabolites excreted by the worms confirming that the majority of NMR signals originated from live worms (supplemental Fig. S4D, E). Viability analysis indicated that most of the worms (>80%) were alive and morphologically indistinguishable from control samples, even at prolonged NMR acquisition times (Fig. 4D, E).

The analysis of the 2D ^1H - ^{13}C HSQC spectrum of live worms revealed signals with chemical shifts values matching lipid species, including those from the olefinic carbons of UFA at ~ 5.35 and 129 ppm in the ^1H and ^{13}C dimensions, respectively. To better

assign those signals, we prepared parallel total lipid extract of the ^{13}C -isotopically enriched worms and directly compared the ID ^{13}C and 2D ^1H - ^{13}C HSQC spectra with those of the live worms (supplemental Fig. S5A, B). While the ID ^{13}C spectrum of live worms show signals from many metabolites such as amino acids, sugars, and other small molecules, it clearly showed a cluster of signals centered at ~ 129 ppm that correspond to the olefinic carbons of UFA (supplemental Fig. S5A, B). The overlay of the 2D ^1H - ^{13}C HSQC spectra confirmed this and allowed the identification of other lipid atoms (supplemental Fig. S5C). This analysis clearly demonstrated that lipid signals were present in the spectrum of live animals. A closer inspection of the 2D ^1H - ^{13}C HSQC spectrum of intact N2 worms, especially in the region

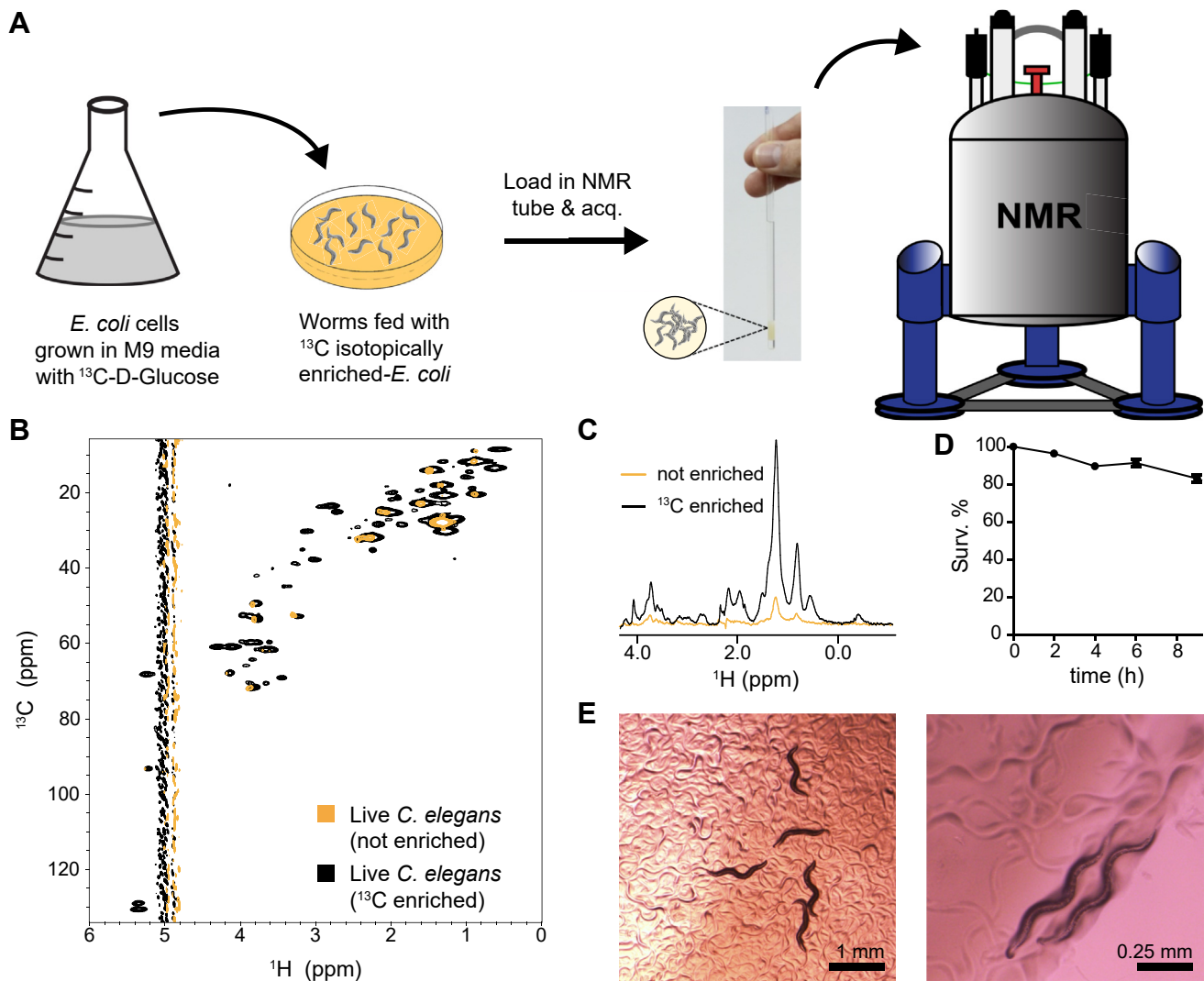


Fig. 4. ^{13}C uniform enrichment and NMR of live *Caenorhabditis elegans*. A: Schematic representation of the protocol for recording 2D ^1H - ^{13}C NMR spectra of live worms uniformly enriched with ^{13}C . B: Overlay of 2D ^1H - ^{13}C HSQC spectra of non-enriched (yellow) and ^{13}C uniformly enriched *C. elegans* (black). C: 1D ^1H spectra obtained from the first ser file of the spectra showed in panel (B). D: Survival percentage of worms in the NMR spectrometer at different acquisition times. E: Bright field images of worms after 4 h at the NMR spectrometer. HSQC, heteronuclear single quantum coherence.

where the glycerol β -backbone signals (-CHOR) appear (~ 5.2 and 70 ppm in ^1H and ^{13}C dimensions, respectively) showed a single cross-peak while the NMR spectra of lipid extracts in that region is characterized by two cross-peaks, one corresponding to TAG and the other to PL (Fig. 5A, left panel). The comparison between the extract and live worm spectra showed that the missing signal corresponds to PL. Analysis of TAG and PL signals in other spectral regions corroborated this (Fig. 5A, right panel and supplemental Fig. S5C), confirming that we do not detect PL in the intact worms. Lipids embedded in membrane assemblies exhibit restricted rotational motions and do not contribute significantly to solution-state NMR spectra (44, 45). Therefore, it is more likely that the detected lipid signals correspond to molecules that tumble more freely in their respective environments and should arise from TAG

and/or free FA. ID ^{13}C analysis in the CO/COO- region of the lipid extract spectra clearly showed signals for esterified acyl chains but not from free carboxylate groups (Fig. 5B) (24), arguing that free FA are scarce in the worms and below the NMR detection limit. Altogether, these evidences strongly suggest that the lipid signals observed in the NMR spectra of live worms correspond to fatty acyl chains esterified in TAG molecules. *C. elegans* store most FA in LD (8), which are mainly composed of TAG, and contain little amounts of sterols and free FA (9). Using Nile red staining and differential fluorescence emission microscopy (38) we confirmed that the worms used in our NMR analysis present large amounts of TAG rich LD while background staining correspond mostly to PL rich, lipid membranes (Fig. 5C). Thus, it seems reasonable to assume that in vivo NMR signals of lipids originate from TAG contained within LD and

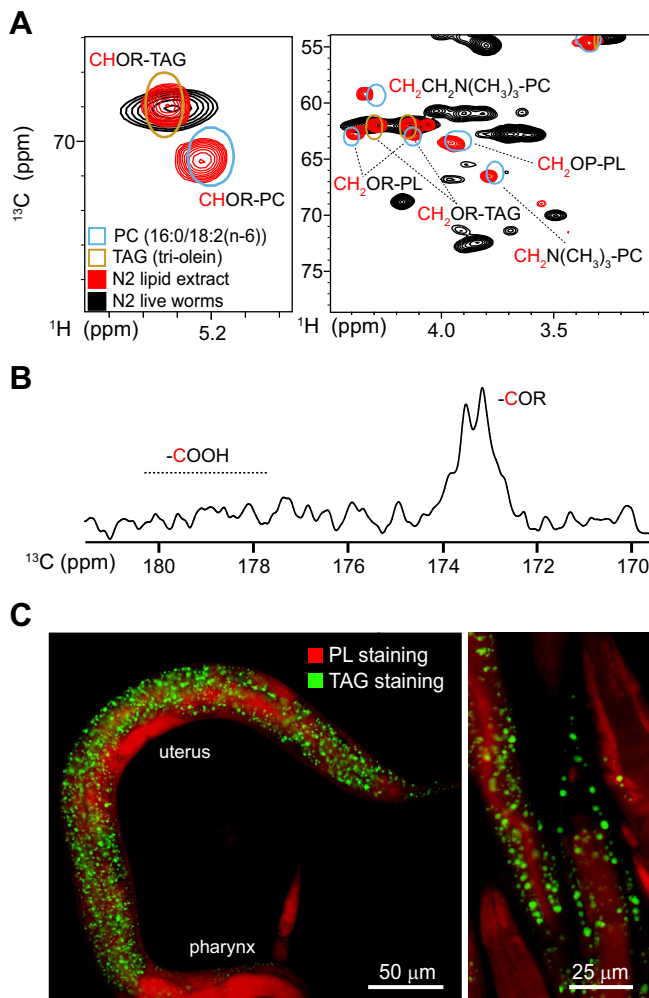


Fig. 5. Lipid NMR detection in live *Caenorhabditis elegans*. A: Overlay of 2D ^1H - ^{13}C HSQC spectra of live, ^{13}C uniformly enriched N2 worms (black), ^{13}C uniformly enriched N2 total chloroform lipid extract (red), triolein (brown), and phosphatidylcholine (cyan), in the TAG/PL regions of the backbone -CHOR (left panel) and other PL and TAG groups (right panel). (B) 1D ^{13}C NMR spectra in the carbonyl and carboxylate region of N2 lipid extract. (C) Fluorescence images of N2 worms stained with Nile Red. Red and green represents polar and neutral lipid staining, respectively. TAG rich lipid droplets are visible as bright green circles. HSQC, heteronuclear single quantum coherence; TAG, triacylglycerols; PL, phospholipids.

that their core is highly fluid and dynamic. This is in agreement with previous studies showing that NMR visible lipid signals in cultured mammalian cells and tissues, referred as mobile lipids, arise from cytosolic LD (46, 47).

Comparative lipid analysis of live N2 and *fat-3* *C. elegans*

To test whether NMR has enough sensitivity and resolution to identify changes in UFA composition in live worms, we performed a comparative analysis of ^{13}C isotopically enriched N2 and *fat-3* animals. The overlay of 1D ^{13}C spectra of N2 and *fat-3* revealed discrete changes in UFA and TAG NMR signals (Fig. 6A, B).

While 1D ^{13}C allowed us to monitor overall changes in different ^{13}C spectral regions of live worm samples, the intrinsic low signal-to-noise ratios and high signal overlap prevents accurate quantifications. Thus, to better analyze these changes we registered 2D ^1H - ^{13}C HSQC spectra of N2 and *fat-3* worms. The spectra of *fat-3* mutants showed a pronounced reduction in the upfield components within the UFA double-bond spectral region (Fig. 6C, D), consistent with the lack of PUFA that rely on intermediates produced by FAT-3. In contrast, the low-field component was higher than those of N2, similar to what we observed in the lipid extract experiments. Thus, our in vivo results clearly show that *fat-3* worms are compromised in PUFA biosynthesis. Replicate experiments on independent samples yielded similar results (supplemental Fig. S6A). In addition to PUFA, we also detected changes in a small number of non-PUFA signals, including TAG. Integration and calculation of the volume ratios between *fat-3* and N2 signals confirmed that total UFA levels were higher while PUFA and TAG content was lower in the *fat-3* animals (Fig. 6E). We also noted higher levels of the - CH_2CO resonance in *fat-3* worms, although the variability of that signal was higher, maybe due to minor contributions of other metabolites in that spectral region. Finally, we set to record semi-selective NMR experiments in the UFA region of live *C. elegans*. Live worms are uniformly labeled with ^{13}C , hence homonuclear ^{13}C coupling results in signal splitting and spectral crowding. To avoid this, we used selective ^{13}C excitation in the UFA region coupled with real-time homonuclear decoupling as reported recently (40). Comparison of the semiselective ^1H - ^{13}C HSQC spectrum of a ^{13}C uniformly enriched N2 extract with one obtained previously at natural abundance showed similar chemical shifts for UFA signals, indicating that ^{13}C labeling and decoupling did not interfere substantially with the NMR detection of UFA acyl chains (supplemental Fig. S7A, B). Next, we registered these experiments with live N2 and *fat-3* worms (Fig. 6F). Despite the inherently broader lines due to field inhomogeneities and viscosity effects, we were able to detect changes between N2 and *fat-3* worms. As observed in the previous experiments, the spectra of *fat-3* worms showed changes mostly in the upfield component of the UFA signals. This was most evident for the set of resonances corresponding to AA and EPA, at 128.7 ppm in the ^{13}C dimension that were present in N2 and vanished in the *fat-3* sample. Overall, these NMR results show that NMR is useful for detecting changes in lipid pools in intact animals.

DISCUSSION

In this work, we used high-resolution heteronuclear NMR methods to analyze the composition of UFA in lipid extracts and in live *C. elegans*. While detection of natural abundance ^{13}C is feasible in cell-free extracts,

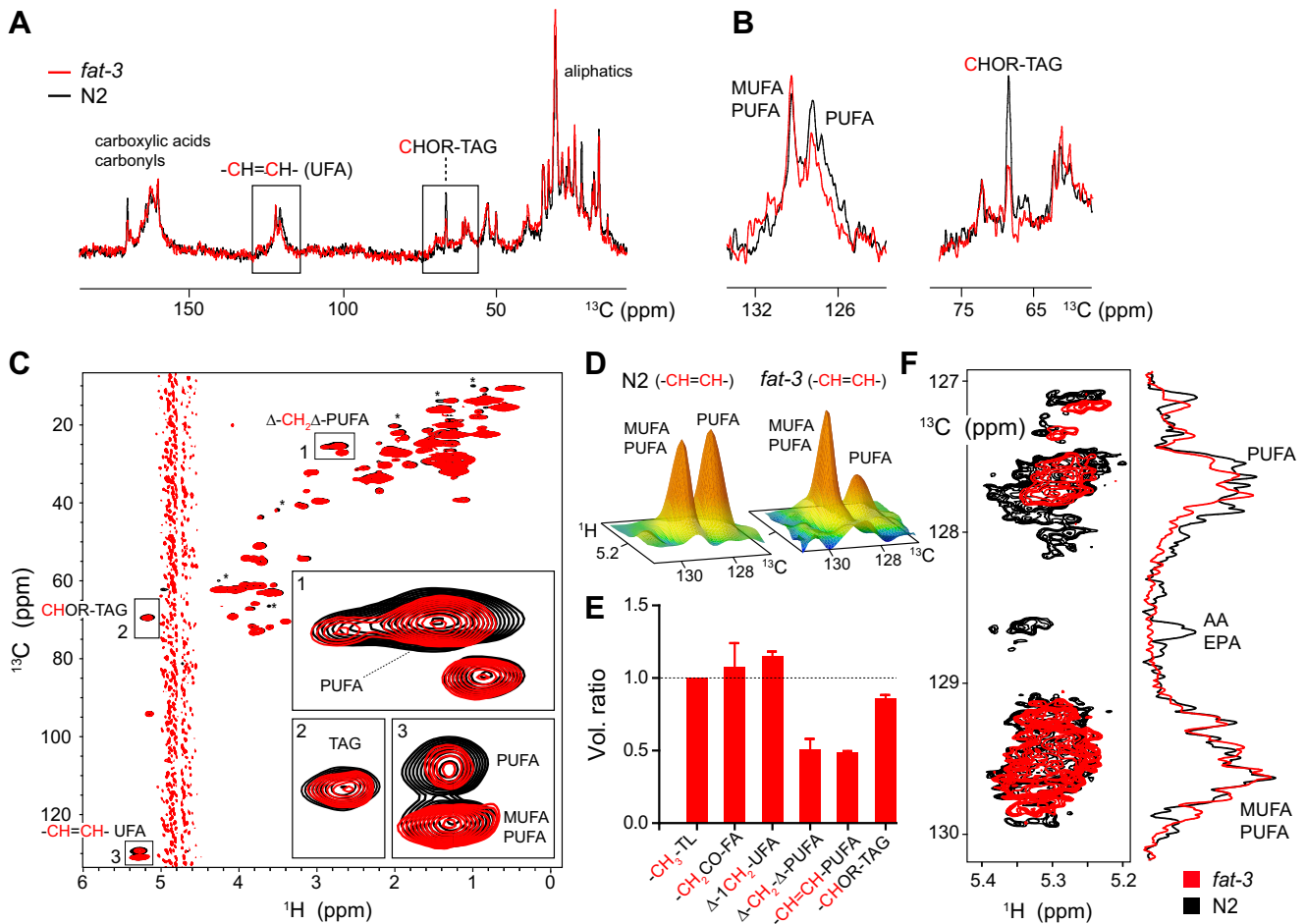


Fig. 6. NMR lipid analysis of live N2 and *fat-3* worms. A: Overlay of 1D ^{13}C NMR spectra of ^{13}C uniformly enriched N2 (black) and *fat-3* (red) live *C. elegans*. The spectral region corresponding to the olefinic atoms of UFA and the -CHOR from the glycerol backbone of TAG and PL are squared and enlarged in panel (B). C: 2D ^1H - ^{13}C HSQC spectra of ^{13}C uniformly enriched N2 (black) and *fat-3* (red) *C. elegans*. Numbered boxes indicate the signals of atoms from different lipids and are enlarged in the individual inset panels. These correspond to the bis-allylic CH_2 groups ($\Delta\text{-CH}_2\text{-}\Delta\text{-PUFA}$) (region 1), the backbone -CHOR group of TAG and PL (region 2) and the olefinic CH groups of UFA (-CH=CH- UFA) (region 3). D: 3D representation of the spectral region corresponding to the olefinic CH groups of UFA (-CH=CH- UFA) (region 3) for N2 (left) and *fat-3* (right) worms. E: Cross-peak volume ratio between *fat-3* and N2 *C. elegans* lipid signals. Bar graph represents mean and std. dev. of two determinations on independent samples. F: Semiselective 2D ^1H - ^{13}C HSQC spectra registered in the (-CH=CH- UFA) (region 3) of N2 (black) and *fat-3* (red) worms. NMR Projections in the ^{13}C dimension from the spectra of N2 and *fat-3* are shown on the right. Asterisks denote minor changes in signals from other metabolites. UFA, unsaturated fatty acids; HSQC, heteronuclear single quantum coherence; TAG, triacylglycerols; PL, phospholipids.

the sensitivity is too low to permit the acquisition of spectra with high signal-to-noise ratios in short periods of time. Thus, ^{13}C uniform isotope labeling is more convenient to perform the in vivo experiments. In addition, field inhomogeneities due to the presence of live worms in the NMR tube and increased viscosity in the cellular environment results in severe ^1H LB which hampers accurate signal identification and analysis using only proton NMR. ^{13}C is less sensitive than ^1H to these conditions and combined with the use in 2D heteronuclear routines increases spectra resolution substantially. NMR spectroscopy is non-destructive, provides high-resolution structural information of biomolecules and is quantitative, thus permitting the identification and quantification of lipids in vitro and in native environments. We assigned the lipid pool of *C. elegans* and identified differences between N2 and *fat-*

3 worms that were consistent with the lack of $\Delta 6$ fatty desaturase activity in the mutant animals. Hence, NMR offers a complementary readout to previously established analytical techniques for lipid analysis in *C. elegans*, such as TLC, GC, or LC-MS with the benefit of accessing the information in live animals with high resolution. Currently, there are few methodologies to study lipid contents in live *C. elegans*. Fluorescence microscopy coupled to lipophilic dyes enables the spatial analysis of lipid distributions within body tissue and discrimination of neutral and charged lipids (38, 48). Other imaging methodologies, such as CARS, were put forward to characterize the distribution of lipids across the body of live *C. elegans*, including the size and content of LD, in a label-free manner (13–15). Compared to these methodologies, our approach has enticing advantages because it enables the identification of lipids in intact animals,

the individual analysis of different lipid classes, i.e. free FA, TAG, and UFA acyl chains, and a comparative assessment of FA unsaturation levels. Furthermore, we provide compelling evidence that the detected lipid molecules correspond to lipid stores within *C. elegans* LD. LD store lipid molecules that are available to sustain cellular metabolism and the biosynthesis of membranes, hormones, and lipoproteins (49). They also play fundamental roles in trafficking of lipids and proteins (50) and protect from lipotoxicity by accumulating excess of free FA and TAG (51). LD functions are modulated by their composition and structure (52, 53), thus the NMR investigation of LD in vivo may provide important new insights linking lipid metabolism, cellular function, and whole organism behavior.

As mentioned, our NMR routine permits the comparative characterization of FA unsaturation levels in live N2 and mutant *C. elegans*. Indeed, we confirmed that *fat-3* worms contained fewer amounts of PUFA. This was particularly clear for C20 PUFA, AA, and EPA, which present isolated, clustered NMR signals in the semiselective ^1H - ^{13}C HSQC spectra. We also detected changes in other signals, including a reduction in TAG levels that were consistent with the lipid quantifications performed initially in worm chloroform extracts, suggesting that FAT-3 may be interconnected with other metabolic routes and/or that the deficiency of long-chain PUFA modified the biosynthesis and/or storage of lipids and other metabolites. Interestingly, CARS scattering microscopy studies of body lipids in N2 and *fat-3* worms revealed similar size and distribution of LD although *fat-3* displayed a ~20% reduction of TL content in the LD (54). These data agree with the lower amounts of TAG we observed in *fat-3* mutants and further support the notion that the lipids we are detecting by NMR are stored in LD.

Here, we studied WT and a mutant worm with inactive FAT-3 and FAT-4 lipid desaturase enzymes. These strains were chosen because PUFA biosynthesis is interrupted at different stages across the biosynthetic pathway, producing lipid mixtures containing both ω 3 and ω 6 PUFA (7). In particular, these worms do not synthesize AA which is a pivotal molecule for many signaling pathways, including the biosynthesis of the endocannabinoids 2-arachidonoylglycerol (2-AG) and N-arachidonylethanolamine (anandamide, AEA). These molecules regulate cholesterol homeostasis in *C. elegans* and in mammalian astrocytes (36, 55) and a plethora of other biological pathways in humans including the control of the endocrine system, food intake, hematopoiesis, and embryo development (56). Thus, monitoring PUFA metabolism in vivo and under varying experimental conditions may shed light on the biosynthesis of endocannabinoids and its effects on *C. elegans* development and physiology, setting benchmarks to understand these processes in human cells.


This methodology may be useful for studying the role of other important desaturases in live *C. elegans*,

such as FAT-1 that is unable to produce ω 3 FA (7) or FAT-2 which does not have PUFA (7) and has perturbed LD metabolism (54, 57). Here, we performed the lipid analysis in synchronized animals at the L4 stage, but these methods may be used to study lipid composition and dynamics at earlier developmental stages, such as L1 or L2. However in this case the number of worms that should be loaded in the NMR tube is higher due to their smaller size. NMR of live worms should also permit the study of different environmental conditions, such as dietary regimes, pharmacological treatments, and/or the use of other genetic mutants that influence lipid homeostasis. In addition, the atomic resolution attainable by solution state NMR of ^{13}C -isotopically enriched, intact worms indicates that these type of analysis is not solely for lipids but has broad applications to other metabolites such as sugars, amino acids, and other small compounds (31). The non-destructive nature of NMR, and the fast acquisition times enabled by the introduction of ^{13}C isotopic enrichment permits the real-time visualization of individual biomolecules in live worms and the monitoring of their cellular interconversions under different biological conditions, as recently shown (31). It should be noted that these applications are limited by the sensitivity of NMR spectroscopy. The detection limit of a typical NMR metabolomics study is $\sim 1 \mu\text{M}$, a 100 times higher compared to LC-MS (58). Furthermore, NMR detection of biomolecules in live worms is more challenging than in cell-free extracts, as field inhomogeneities, viscosity effects, signal overlapping, and the need to introduce multiple spectral dimensions results in higher detection limits. That means that in vivo NMR typically accesses the primary cellular metabolism, i.e. those molecules that are present at high concentration, and fails to detect low concentrated metabolites. However, the development of more sensitive NMR hardware, fast acquisition and non-uniform sampling schemes may decrease the detection limits substantially (59, 60).

Many of the open questions in lipid-metabolism research are directly linked to human diseases and analytical methods to address these questions are in great demand. *C. elegans* is a model for which there is a vast array of genetic, biochemical, and molecular biology tools available to introduce changes in protein expression, gene silencing, or overexpression resulting in perturbations at different positions of the animal metabolism. NMR spectroscopy of isotopically enriched *C. elegans* enables high-resolution characterization of lipid compositions in specific sub-anatomical distributions, such as LD. Imaging studies complement this by providing spatial characterization of these structures. Since NMR spectroscopy is non-destructive, it allows for the direct correlation of lipid metabolism with phenotypic or behavioral analyses in live animals. We are currently using these integrated approaches to

study the role of lipid metabolism in the onset of neurodegenerative diseases like Parkinson's and Niemann-Pick diseases, as well as in fertility and development processes where lipid metabolism plays a central role. We anticipate that combining these methodologies will offer unparalleled insights into lipid storage and the activities of enzymes involved in FA metabolism under both physiological and pathological conditions, potentially identifying new targets for pharmacological intervention.

Data Availability

All relevant data are included in the article and its supporting information. 

Supplemental data

This article contains [supplemental data](#).


Acknowledgments

We acknowledge Philipp Selenko and Alejandro J. Vila for reading and commenting on the manuscript, Andrea Coscia and Alejandro Gago for maintenance of the NMR infrastructure, Cecilia Vranych for assistance with *C. elegans* growth and maintenance and Eleonora García-Vescovi and Guillermo Labadie for providing pure linoleic and arachidonic acids.

Author contributions

B. H. C., G. P., V. A. L., F. V. G., C. B. D., S. A., D. d. M., and A. B. investigation; B. H. C., G. P., V. A. L., S. A., D. d. M., and A. B. visualization; B. H. C., G. P., V. A. L., F. V. G., C. B. D., S. A., D. d. M., and A. B. formal analysis; B. H. C., G. P., D. d. M., and A. B. methodology; B. H. C., G. P., V. A. L., F. V. G., C. B. D., and S. A. writing–review and editing; S. A., D. d. M., and A. B. resources; D. d. M. and A. B. writing–original draft; D. d. M. and A. B. supervision; D. d. M. and A. B. project administration; D. d. M. and A. B. conceptualization; D. d. M. and A. B. funding acquisition.

Author ORCIDs

Florencia V. Guastaferrri  <https://orcid.org/0009-0008-1394-2618>

Andres Binolfi  <https://orcid.org/0000-0003-2374-0864>

Funding and additional information

This work was funded by CONICET, Agencia I+D+i (PICT-2018-02572 to A. B. and D. d. M.) and the Richard Lounsbery Foundation (to A. B. and D. d. M.).

Conflict of interest

The authors declare that they have no conflicts of interest with the contents of this article.

Abbreviations

AA, arachidonic acid; ALA, α -linolenic acid; CARS, Coherent anti-Stokes Raman spectroscopy; DGLA, dihommo- γ -linoleic acid; EM, exponential multiplication; EPA, eicosapentanoic acid; FA, fatty acids; FAME, fatty acid methyl ester; *fat-3*, $\Delta 6$ fatty acid desaturase, gene/mutant strain; FAT-3, $\Delta 6$ fatty acid desaturase protein; *fat-4*, $\Delta 5$ fatty

acid desaturase, gene/mutant strain; FAT-4, $\Delta 5$ fatty acid desaturase protein; HSQC, heteronuclear single quantum coherence; LA, linoleic acid; LB, line broadening; LD, lipid droplets; MUFA, monounsaturated fatty acids; NGM, nematode growth medium; PL, phospholipids; PUFA, polyunsaturated fatty acids; SW, spectra width; TAG, triacylglycerols; TL, total lipids, methyl signal; UFA, unsaturated fatty acids.

Manuscript received February 28, 2024, and in revised form August 5, 2024. Published, JLR Papers in Press, August 8, 2024, <https://doi.org/10.1016/j.jlr.2024.100618>

REFERENCES

1. de Carvalho, C., and Caramujo, M. J. (2018) The various roles of fatty acids. *Molecules* **23**, 2583
2. Gianfrancesco, M. A., Paquot, N., Piette, J., and Legrand-Poels, S. (2018) Lipid bilayer stress in obesity-linked inflammatory and metabolic disorders. *Biochem. Pharmacol.* **153**, 168–183
3. Heron, M. (2013) Deaths: leading causes for 2010. *Natl. Vital Stat. Rep.* **62**, 1–96
4. Fanning, S., Haque, A., Imberdis, T., Baru, V., Barrasa, M. I., Nuber, S., et al. (2019) Lipidomic analysis of alpha-synuclein neurotoxicity identifies stearyl CoA desaturase as a target for Parkinson treatment. *Mol. Cell.* **73**, 1001–1014.e1008
5. Watts, J. L., and Ristow, M. (2017) Lipid and carbohydrate metabolism in *Caenorhabditis elegans*. *Genetics* **207**, 413–446
6. Watts, J. L. (2016) Using *Caenorhabditis elegans* to uncover conserved functions of omega-3 and omega-6 fatty acids. *J. Clin. Med.* **5**, 19
7. Watts, J. L., and Browse, J. (2002) Genetic dissection of polyunsaturated fatty acid synthesis in *Caenorhabditis elegans*. *Proc. Natl. Acad. Sci. U. S. A.* **99**, 5854–5859
8. Mak, H. Y. (2012) Lipid droplets as fat storage organelles in *Caenorhabditis elegans*: thematic review series: lipid droplet synthesis and metabolism: from yeast to man. *J. Lipid Res.* **53**, 28–33
9. Vrablik, T. L., Petyuk, V. A., Larson, E. M., Smith, R. D., and Watts, J. L. (2015) Lipidomic and proteomic analysis of *Caenorhabditis elegans* lipid droplets and identification of ACS-4 as a lipid droplet-associated protein. *Biochim. Biophys. Acta.* **1851**, 1337–1345
10. Papsdorf, K., Miklas, J. W., Hosseini, A., Cabruja, M., Morrow, C. S., Savini, M., et al. (2023) Lipid droplets and peroxisomes are co-regulated to drive lifespan extension in response to monounsaturated fatty acids. *Nat. Cell Biol.* **25**, 672–684
11. Witting, M., and Schmitt-Kopplin, P. (2016) The *Caenorhabditis elegans* lipidome: a primer for lipid analysis in *Caenorhabditis elegans*. *Arch. Biochem. Biophys.* **589**, 27–37
12. Escorcía, W., Ruter, D. L., Nhan, J., and Curran, S. P. (2018) Quantification of lipid abundance and evaluation of lipid distribution in *Caenorhabditis elegans* by Nile red and oil red O staining. *J. Vis. Exp.* **133**, 57352
13. Chen, T., Yavuz, A., and Wang, M. C. (2022) Dissecting lipid droplet biology with coherent Raman scattering microscopy. *J. Cell Sci.* **135**, jcs252353
14. Chen, W. W., Lemieux, G. A., Camp, C. H., Jr., Chang, T. C., Ashrafi, K., and Cicerone, M. T. (2020) Spectroscopic coherent Raman imaging of *Caenorhabditis elegans* reveals lipid particle diversity. *Nat. Chem. Biol.* **16**, 1087–1095
15. Hellerer, T., Axang, C., Brackmann, C., Hillertz, P., Pilon, M., and Enejder, A. (2007) Monitoring of lipid storage in *Caenorhabditis elegans* using coherent anti-Stokes Raman scattering (CARS) microscopy. *Proc. Natl. Acad. Sci. U. S. A.* **104**, 14658–14663
16. Sedman, J., Gao, L., Garcia-Gonzalez, D., Ehsan, S., and van de Voort, F. R. (2010) Determining nutritional labeling data for fats and oils by ^1H NMR. *Eur. J. Lipid Sci. Technol.* **112**, 439–451
17. Thoss, V., Murphy, P. J., Marriott, R., and Wilson, T. (2012) Triacylglycerol composition of British bluebell (*Hyacinthoides non-scripta*) seed oil. *RSC Adv.* **2**, 5314–5322
18. Knothe, G., and Kenar, J. A. (2004) Determination of the fatty acid profile by ^1H -NMR spectroscopy. *Eur. J. Lipid Sci. Technol.* **106**, 88–96

19. Amiel, A., Tremblay-Franco, M., Gautier, R., Ducheix, S., Montagner, A., Polizzi, A., *et al.* (2019) Proton NMR enables the absolute quantification of aqueous metabolites and lipid classes in unique mouse liver samples. *Metabolites* **10**, 9
20. Willker, W., and Leibfritz, D. (1998) Assignment of mono- and polyunsaturated fatty acids in lipids of tissues and body fluids. *Mag. Res. Chem.* **36**, S79–S84
21. Oostendorp, M., Engelke, U. F., Willemsen, M. A., and Wevers, R. A. (2006) Diagnosing inborn errors of lipid metabolism with proton nuclear magnetic resonance spectroscopy. *Clin. Chem.* **52**, 1395–1405
22. Mika, A., Kaczynski, Z., Stepnowski, P., Kaczor, M., Proczko-Stepaniak, M., Kaska, L., *et al.* (2017) Potential application of (1)H NMR for routine serum lipidome analysis -evaluation of effects of bariatric surgery. *Sci. Rep.* **7**, 15530
23. Baumstark, D., Kremer, W., Boettcher, A., Schreier, C., Sander, P., Schmitz, G., *et al.* (2019) (1)H NMR spectroscopy quantifies visibility of lipoproteins, subclasses, and lipids at varied temperatures and pressures. *J. Lipid Res.* **60**, 1516–1534
24. Alexandri, E., Ahmed, R., Siddiqui, H., Choudhary, M. I., Tsiafoulis, C. G., and Gerothanassis, I. P. (2017) High resolution NMR spectroscopy as a structural and analytical tool for unsaturated lipids in solution. *Molecules* **22**, 1663
25. Tesiram, Y. A., Saunders, D., and Towner, R. A. (2008) Chemical speciation by selective heteronuclear single-quantum coherence spectroscopy: determination of double-bond quantity in unsaturated fatty acid compounds. *NMR Biomed.* **21**, 345–356
26. Lane, D., Skinner, T. E., Gershenson, N. I., Bermel, W., Soong, R., Dutta Majumdar, R., *et al.* (2019) Assessing the potential of quantitative 2D HSQC NMR in (13)C enriched living organisms. *J. Biomol. NMR* **73**, 31–42
27. Lane, D., Soong, R., Bermel, W., Ning, P., Dutta Majumdar, R., Tabatabaei-Anaraki, M., *et al.* (2019) Selective amino acid-only in vivo NMR: a powerful tool to follow stress processes. *ACS Omega* **4**, 9017–9028
28. Sanchez-Lopez, C., Labadie, N., Lombardo, V. A., Biglione, F. A., Manta, B., Jacob, R. S., *et al.* (2020) An NMR-based biosensor to measure stereospecific methionine sulfoxide reductase activities in vitro and in vivo. *Chem. Eur. J.* **26**, 14838–14843
29. Thole, J. F., Fadero, T. C., Bonin, J. P., Stadtmiller, S. S., Giudice, J. A., and Pielak, G. J. (2021) Danio rerio oocytes for eukaryotic in-cell NMR. *Biochemistry* **60**, 451–459
30. Lombardo, V. A., Armesto, R., Herrera-Estrada, I., and Binolfi, A. (2023) High resolution protein in-cell NMR in zebrafish embryos. *J. Magn. Res. Open* **16–17**, 100111
31. Nguyen, T. T. M., An, Y. J., Cha, J. W., Ko, Y. J., Lee, H., Chung, C. H., *et al.* (2020) Real-time in-organism NMR metabolomics reveals different roles of AMP-activated protein kinase catalytic subunits. *Anal. Chem.* **92**, 7382–7387
32. Brenner, S. (1974) The genetics of *Caenorhabditis elegans*. *Genetics* **77**, 71–94
33. Schachat, F., Garcea, R. L., and Epstein, H. F. (1978) Myosins exist as homodimers of heavy chains: demonstration with specific antibody purified by nematode mutant myosin affinity chromatography. *Cell* **15**, 405–411
34. Fabian, T. J., and Johnson, T. E. (1994) Production of age-synchronous mass cultures of *Caenorhabditis elegans*. *J. Gerontol.* **49**, B145–B156
35. Folch, J., Lees, M., and Sloane Stanley, G. H. (1957) A simple method for the isolation and purification of total lipides from animal tissues. *J. Biol. Chem.* **226**, 497–509
36. Galles, C., Prez, G. M., Penkov, S., Boland, S., Porta, E. O. J., Altabe, S. G., *et al.* (2018) Endocannabinoids in *Caenorhabditis elegans* are essential for the mobilization of cholesterol from internal reserves. *Sci. Rep.* **8**, 6398
37. Pino, E. C., Webster, C. M., Carr, C. E., and Soukas, A. A. (2013) Biochemical and high throughput microscopic assessment of fat mass in *Caenorhabditis elegans*. *J. Vis. Exp.* **73**, 50180
38. Schnitzler, J. G., Bernelot Moens, S. J., Tiessens, F., Bakker, G. J., Dallinga-Thie, G. M., Groen, A. K., *et al.* (2017) Nile Red Quantifier: a novel and quantitative tool to study lipid accumulation in patient-derived circulating monocytes using confocal microscopy. *J. Lipid Res.* **58**, 2210–2219
39. Schneider, C. A., Rasband, W. S., and Eliceiri, K. W. (2012) NIH Image to ImageJ: 25 years of image analysis. *Nat. Methods* **9**, 671–675
40. Bodor, A., Haller, J. D., Bouguechtouli, C., Theillet, F. X., Nyitray, L., and Luy, B. (2020) Power of pure shift HalphaAlpha correlations: a way to characterize biomolecules under physiological conditions. *Anal. Chem.* **92**, 12423–12428
41. Hwang, T. L., and Shaka, A. J. (1998) Water suppression that works. Excitation sculpting using arbitrary wave-forms and pulsed-field gradients. *J. Magn. Reson.* **112**, 275–279
42. Sparling, M. L., Zidovetzki, R., Muller, L., and Chan, S. I. (1989) Analysis of membrane lipids by 500 MHz 1H NMR. *Anal. Biochem.* **178**, 67–76
43. Goddard, T. D., and Kneller, D. G. (2002) Sparky 3. University of California, San Francisco
44. Griffin, R. G. (1981) Solid state nuclear magnetic resonance of lipid bilayers. *Methods Enzymol.* **72**, 108–174
45. Hakumaki, J. M., and Kauppinen, R. A. (2000) 1H NMR visible lipids in the life and death of cells. *Trends Biochem. Sci.* **25**, 357–362
46. Barba, I., Cabanas, M. E., and Arus, C. (1999) The relationship between nuclear magnetic resonance-visible lipids, lipid droplets, and cell proliferation in cultured C6 cells. *Cancer Res.* **59**, 1861–1868
47. Perez, Y., Lahrech, H., Cabanas, M. E., Barnadas, R., Sabes, M., Remy, C., *et al.* (2002) Measurement by nuclear magnetic resonance diffusion of the dimensions of the mobile lipid compartment in C6 cells. *Cancer Res.* **62**, 5672–5677
48. Elle, I. C., Olsen, L. C., Pultz, D., Rodkaer, S. V., and Faergeman, N. J. (2010) Something worth dyeing for: molecular tools for the dissection of lipid metabolism in *Caenorhabditis elegans*. *FEBS Lett.* **584**, 2183–2193
49. Pol, A., Gross, S. P., and Parton, R. G. (2014) Review: biogenesis of the multifunctional lipid droplet: lipids, proteins, and sites. *J. Cell Biol.* **204**, 635–646
50. Murphy, D. J. (2012) The dynamic roles of intracellular lipid droplets: from archaea to mammals. *Protoplasma* **249**, 541–585
51. Olzmann, J. A., and Carvalho, P. (2019) Dynamics and functions of lipid droplets. *Nat. Rev. Mol. Cell Biol.* **20**, 137–155
52. Henne, W. M. (2023) The (social) lives, deaths, and biophysical phases of lipid droplets. *Curr. Opin. Cell Biol.* **82**, 102178
53. Rogers, S., Gui, L., Kovalenko, A., Zoni, V., Carpentier, M., Ramji, K., *et al.* (2022) Triglyceride lipolysis triggers liquid crystalline phases in lipid droplets and alters the LD proteome. *J. Cell Biol.* **221**, e202205053
54. Yi, Y. H., Chien, C. H., Chen, W. W., Ma, T. H., Liu, K. Y., Chang, Y. S., *et al.* (2014) Lipid droplet pattern and nondroplet-like structure in two fat mutants of *Caenorhabditis elegans* revealed by coherent anti-Stokes Raman scattering microscopy. *J. Biomed. Opt.* **19**, 011011
55. Allende, L. G., Natali, L., Cragolini, A. B., Bollo, M., Musri, M. M., de Mendoza, D., *et al.* (2024) Lysosomal cholesterol accumulation in aged astrocytes impairs cholesterol delivery to neurons and can be rescued by cannabinoids. *Glia* **72**, 1746–1765
56. Salzet, M., Breton, C., Bisogno, T., and Di Marzo, V. (2000) Comparative biology of the endocannabinoid system possible role in the immune response. *Eur. J. Biochem.* **267**, 4917–4927
57. Wang, Y., Li, C., Zhang, J., Xu, X., Fu, L., Xu, J., *et al.* (2022) Polyunsaturated fatty acids promote the rapid fusion of lipid droplets in *Caenorhabditis elegans*. *J. Biol. Chem.* **298**, 102179
58. Emwas, A. H., Roy, R., McKay, R. T., Tenori, L., Saccenti, E., Gowda, G. A. N., *et al.* (2019) NMR spectroscopy for metabolomics research. *Metabolites* **9**, 123
59. Chandra, K., Al-Harhi, S., Sukumaran, S., Almulhim, F., Emwas, A. H., Atreya, H. S., *et al.* (2021) NMR-based metabolomics with enhanced sensitivity. *RSC Adv.* **11**, 8694–8700
60. Zhang, B., Powers, R., and O'Day, E. M. (2020) Evaluation of non-uniform sampling 2D (1)H-(13)C HSQC spectra for semi-quantitative metabolomics. *Metabolites* **10**, 203